Beam Optics of the RRL Cesium Beam Primary Frequency Standard

Koji NAKAGIRI, Haruo OKAZAWA and Shinji URABE

Radio Research Laboratory
Ministry of Posts and Telecommunications
4-2-1, Nukui-Kitamachi, Koganei
Tokyo, 184 JAPAN

ABSTRACT

The laboratory type cesium beam frequency standard, Cs 1, of RRL (Radio Research Laboratory) features a hexapole magnet focusing system, a 55 cm Ramsey cavity using a coaxial line-to-waveguide transducer and a digital servo system.

The length of the Ramsey cavity is relatively short. Therefore, in order to secure a good signal-to-noise ratio, beam uniformity and, to decrease the pulling effect caused by the wings of neighboring field-dependent transitions, a calculation of the beam trajectory, using the Runge-Kutta method, was carried out. In the calculation, the following items were considered: 1) a beam collimator having a finite area instead of a point source, 2) dependence of the effective dipole moment on the position in the magnet, 3) motion of the atoms in the Ψ direction.
After evaluating the equations, the technical advantage of the focusing system using the hexapole magnets became clear. The results of the calculation agreed fairly well with that of the experiment. This recent optimization of the beam optics has probably improved the microwave power dependent frequency shift in the accuracy evaluation of RRL Cs 1.

INTRODUCTION

The laboratory type cesium beam frequency standard, Cs 1, of RRL features a hexapole magnet focusing system, a 55-cm Ramsey cavity using a coaxial line-to-waveguide transducer and a digital servo system[1,2,3,4,5].

A number of accuracy evaluation experiments have been made and the total uncertainty of those evaluations has been gradually lowered because of our efforts towrd various kinds of improvement. After realizing a slow velocity beam optics using hexapole magnets of 3 cm in length with a collimator of 0.5 mm in diameter, the microwave dependent shift was much improved and the total uncertainty of 1.1×10^{-13} was obtained[6]. Then RRL started reporting the data to the BIH. There were, however, many problems remaining unsolved and the possible solutions to them could not be obtained clearly. Therefore, a calculation of beam trajectory for the optimization of the beam optics was carried out and the beam optics and the electronic circuits of the RRL Cs 1 were improved. The magnetic field effect, the pulling by the neaighboring transitions and the power dependent shifts were studied experimentally and theoretically[7]. The total uncertainty of 0.7×10^{-13} was achieved as expected in April, 1986.

In the following, a calculation of beam trajectory for the optimization of beam optics is explained and the results of calculation are compared with those of experiment.

CALCULATION

The magnetic potential in the region between the pole-pieces of hexapole magnet is given by[8]

$$V=Cr^3\cos 3\psi \tag{1}$$

where the cylindrical coordinate(r, ψ, z) is adopted and z coordinate is made to coincide with the center axis of the hexapole magnet. The magnetic field in the r and the ψ directions can be written as gradient of Eq. (1)

$$H_r=-H_{max}(r/r_o)^2\cos 3\psi \tag{2}$$

$$H_\psi=H_{max}(r/r_o)^2\sin 3\psi \tag{3}$$

$$|H|=\sqrt{H_r^2+H_\psi^2} \longrightarrow H_{max} \quad \text{at } r=r_o \tag{4}$$

are obtained, where r_o is a radius of the inscribed circle of hexapole magnet. The force on the atom has the components,

$$F_r=m[d^2r/dt^2-r(d\psi/dt)^2] \tag{5}$$

$$F_\psi=ml/r\frac{d}{dt}(r^2d\psi/dt) \tag{6}$$

where m is the mass of atom. The interaction energy is given by Eq. (4)

$$U=\mu\cdot H=\mu_{eff}\cdot|H|=\mu_{eff}\cdot H_{max}(r/r_o)^2 \tag{7}$$

where μ is the magnetic dipole moment. The interaction energy is a scalar potential, so that

$$F=-\nabla U=\mu_{eff}\cdot\frac{\partial}{\partial r}H_{max}(r/r_o)^2 \tag{8}$$

where $\hat{\imath}$ is the unit vector of the r direction. Eq. (5) and Eq. (6) can be written as

$$m[d^2r/dt^2-r(d\psi/dt)^2]=\mu_{eff}\cdot\frac{2H_{max}}{r^2}\cdot r \tag{9}$$

$$\frac{d}{dt}(r^2d\psi/dt)=0 \tag{10}$$

The effective dipole moment is a function of H and has a different value for each state of cesium atom:

$$\mu_{eff}(F=7/2\pm 1/2, m_F) = \frac{x+m_F/4}{2(1+1/2m_Fx+x^2)^{1/2}}(-2\mu_o) \tag{11}$$

where $x=-2\mu_0 \cdot H/ W=-3.052 \times 10^{-4}H$ and H is the magnetic field intensity. It is difficult to solve eqs. (9), (10) and (11) analytically. Therefore they are solved as a group of differential equations (r, $\dot{r}$, Ψ, $\dot{\Psi}$) numerically by the Runge-Kutta method. For example, the numerical values of (r, $\dot{r}$, Ψ, $\dot{\Psi}$) are calculated 30 times for the approximation in the case of the 6 cm magnet. It is assumed that the flight time in each of 30 segments does not vary with the r position, and the motion of the atom under the condition $r<1/10r_0$ is assumed to be the same as that in the free potential space, since the magnetic potential in the region is very small. Hence, the equation can avoid divergence under the condition $r<0$.

In the calculation the beam collimator has finite area instead of a point source and it is assumed that many collimators of a 0.1 mm diameter gather to form a bundle and the directivity[9] of each 0.1 collimator is the same as that of the original one.

OPTIMUM DESIGN OF BEAM OPTICS

Figure 1 shows a velocity dependence of the cesium beam intensity at the exit of the collimator. The intensity ratio of the 100 m/s beam to the most probable velocity 270 m/s beam is 1:6.2. The size of the collimator may be chosen so that the compensation for beam intensity by increase of temperature does not induce poor beam directivity of the collimator. Figure 2 show a r^2 -dependence of the magnetic field intensity between the pole tips of the 6 cm hexapole magnet which was use during the initial phase of the experiment. The inscribed radius is 1.5 mm. In the calculation the effect of deviation from the r^2 law is considered. Figure 3 shows the typical calculation results of velocity distribution in beams using a 6 cm magnet and a 3 cm magnet. One pair of 3 cm magnets was selected for an optimum focusing system, since the microwave power dependent frequency shift was much improved with 3 cm magnets in May 1984. The collimators of 0.5 mm diameter and 1 mm length were used. However, the efficiency of the beam using these collimators was low experimentally. In the design of the beam optics, the following items were considered: 1) beam efficiency for better frequency stability, 2) beam uniformity, which is also influenced by the gravitational force on the atoms, and its effect has a relation to the beam asymmetry in the interaction region of the Ramsey cavity and in the cutoff waveguide, 3) pulling effect by the wings of the neighboring transition ($F=4$, $m_f=\pm1$) to ($F=3$, $m_f=\pm1$).

Figure 4 shows the distribution of arrival of the atoms in the r-direction at the detector for different collimator diameters. The distance between the collimator and the magnet is 2.3 cm and the diameter of the beam stopper is 1.2 mm. In the case of flop-out type detector, Figure 4 indicates that the radii of 0.4 mm, 0.6 mm and 0.75 mm are optimum for the collimators of 0.5 mm, 0.8 mm and 1.0 mm in diameter respectively. Figure 5 shows the velocity distributions for different collimator diameters. The dependence upon the distance between the oven and the collimator is also calculated and the same characteristic, but the dependence of the

probable velocities upon the distance is stronger than that upon the collimator diameter. Figure 6 shows the examples of Ramsey resonance at 3 dB below the optimum power for different collimator diameters. In the case of 0.8 mm collimator diameter, the linewidth and the peak-to-valley of Ramsey resonance at the temperature of 100 °C are 105 Hz and 2.26 pA, respectively. The total number of atoms which arrive at detector without transition is about 7.3 times as many as the number of the ($F=4$, $m_F=0$) energy state for the three different collimators. Figure 7 shows the estimated short term stability and most probable velocity. On the basis of above-mentioned calculations and previous experimental results, the beam optic parameters and dimensions are decided as shown in Figure 8.

EXPERIMENTAL RESULTS AND DISCUSSION

Figure 9 shows the obsereved Rabi transitions at 3 dB below the optimum power. The magnetic field is usually set for 1.088188 T^{-5} in operation. Figure 10 shows the beam current characteristic around the clock transition. Figure 11 shows the Ramsey resonance of clock transition. Its linewidth and peak-to-valley beam current at an oven temperarure of about 112 °C are 100 Hz and 4 pA, respectively. The vapor pressure of 100°C, 112 °C and 140 °C in oven are $0.55X10^{-3}$ mmHg, $0.90X10^{-3}$ mmHg and $2.5X10^{-3}$ mmHg, respectively . Judging from these data and the results in Figure 7, the beam efficiency has been improved 3~4 times, compared with the previous one.

Figure 12 shows the velocity distributions of three transitions, which indicates the reproducibilities in the same and opposite beam directions. The improvement of beam stoppers in their pattern and position adjustment were also effective in these reproducibilities. These results are satisfactory and agree fairly well with the calculated ones, as shown in Figure 5. Figure 13 shows the recent microwave power dependent frequency shift together with the results in the previous experiment. The uncertainty of $0.7X10^{-13}$ is obtained in the accuracy evaluation experiment. It was $1.1X10^{-13}$ in the previous one.

CONCLUSION

The authors have designed the optimum beam optics on the basis of a caluculation using Runge-Kutta method and the previous experimental data. The calculated results agree fairly well with those of the experiment. The obtained improvements in the short term stability and the uncertainty of RRL Cs 1 are satisfactory.

As to the Runge-Kutta method, the authors adopted this to design the beam optics using 6 cm magnets at the initial stage of experiment[1,3] and to design the present beam optics using 3 cm magnets . Huang Bingying of National Institute of Metrology in China also developed this method to design a new cesium standard using hexapole magnets and concluded that this method was useful for the simulation of beam optics[12]. In our calculaton, it is a demerit to take much time to perform a numerical

calculation, for example 15~20 minutes typically. Therefore further improvement for efficient and precise calculation will be desirable.

ACKNOWLEDGMENT

The authors would like to thank Mr. N. Imai for his support and advice. The authors would like to acknowledg the contributions of Mr. J. Umezu, Mr. Ohta and Mr. H. Saito to this work.

REFERENCES

1. M. Kobayashi et al., "Design of and Preliminary results on a Cesium-Beam Standard at the Radio Research Standard at the Radio Research Laboratories, "IEEE Trans. Instrum. Meas. ,IM-27, pp. 343-348, 1978.

2. S. Urabe et al., "Majorana Effect on Atomic Frequency Standards",IEEE Trans.,IM-29, pp. 304-310, 1980.

3. K. Nakagiri et al., "Cesium Beam Frequency Standard at the Radio Reseach Laboratories", Journal de Physique 42(3rd Sym. on Frequency and Metrology), pp. c8-253-256, 1981.

4. K. Nakagiri et al., "Cesium Beam Frequency Standard", Review of the Radio Radio Research Laboratories, Vol. 29, pp. 97-115, 1983(in Japanese).

5. K. Nakagiri et al., "A Squarewave Frequency Modulation Servo System for Cesium Frequency Standard and its influence on Frequency Stability", J. Appl. Phys. Soc. Japan, Vol. 50, pp. 122-130, 1981 (in Japanese).

6. K. Nakagiri et al., "Accuracy Evaluation of the RRL Primary Cesium Beam Standard, "Proc. 38th Annual Sym. on Frequency Control, pp. 447-451, 1984.

7. K. Nakagiri et al., "Studies on Accurate Evaluation of the RRL Primary Frequency Standard", IEEE Trans. ,S-IM, to be published in June, 1987.

8. C. Audoin, "Calcul du Circuit Magnetique Dune Lentille Hexapolaire a Aimants Permanents", Journal de Physique Appliquize, Vol. 26, pp. 71A-76A, 1965.

9. B. B. Dayton, "Gas Flow Pattern at Entrance and Exit of Cylindrical Tubes", 1956 Nath. Sym. Vac. Technol. Trans., pp.5-11, 1957.

10. R. C. Mockler, "Atomic Beam Frequency Standards", Advances in Electronics and Electron Phisics, Vol. 15, pp. 1-71, 1961.

11. H. Damms, "Corrections for Second-Order Doppler Shift and Cavity Phase

Error in Cesium Atomic Beam Frequency", IEEE Trans. IM-23,pp. 509-514, 1974.

12. B. Huang, "A Calculation for Six Pole Cesium Beam Optics", paper presented at Int. Sym. on Time and Frequency, Hanghou, China, 1983.

TITLES OF FIGURES

Fig. 1 Velocity distribution at the exit of collimator.
Fig. 2 r dependence of the magnetic field intensity.
Fig. 3 Typical velocity distributions in beams using 3 cm magnets and 6 cm magnets
Fig. 4 Distributions of the arrival atoms in the radius direction at detector.
Fig. 5 Velocity distribution for different collimator diameters.
Fig. 6 Ramsey resonance for different collimators.
Fig. 7 Estimated short term stability and most probable velocity.
Fig. 8 Improved beam optics and the structure of Ramsey cavity.
Fig. 9 Observed Rabi transitions.
Fig. 10 Beam current arround the clock transition.
Fig. 11 Ramsey resonance of the clock transition.
Fig. 12 Velocity distribution of three transitions.
Fig. 13 Microwave power dependent characteristic on beam reversal, compared with that in the previous optics.

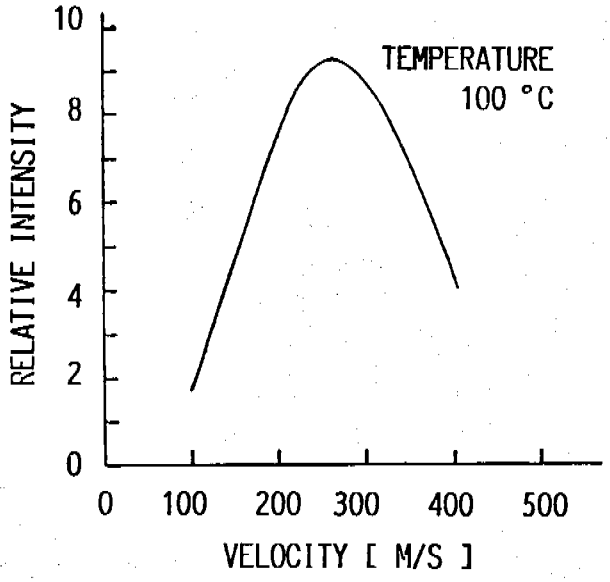

Fig. 1 Velocity distribution at the exit of collimator.

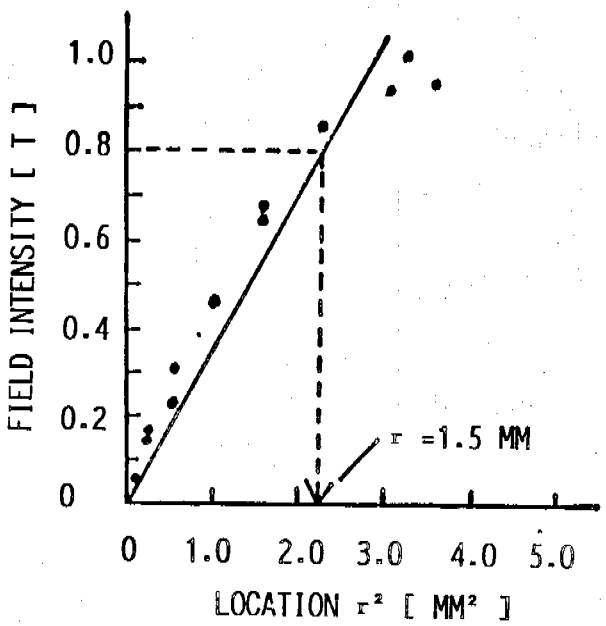

Fig. 2 r^2 dependence of the magnetic field intensity.

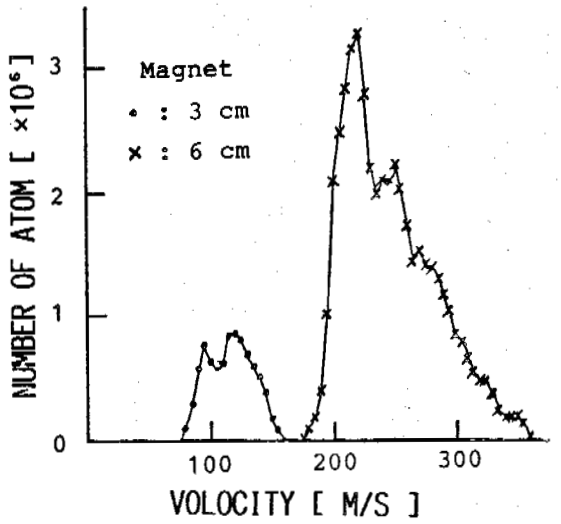

Fig. 3 Typical velocity distributions in beams using 3 cm magnets and 6 cm magnets

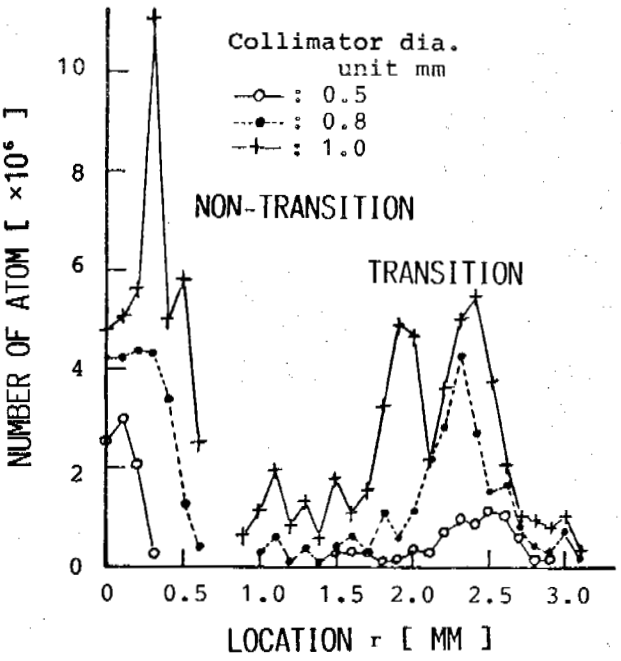

Fig. 4 Distributions of the arrival atoms in the radius direction at detector.

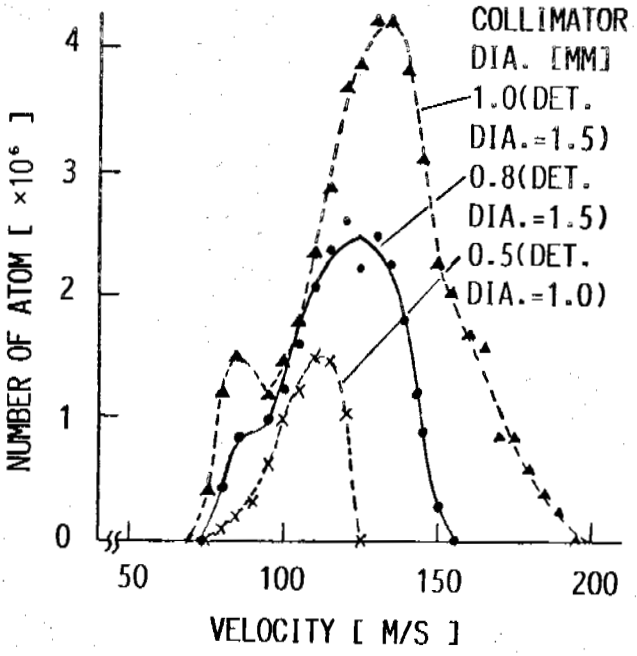

Fig. 5 Velocity distribution for different collimator diameters.

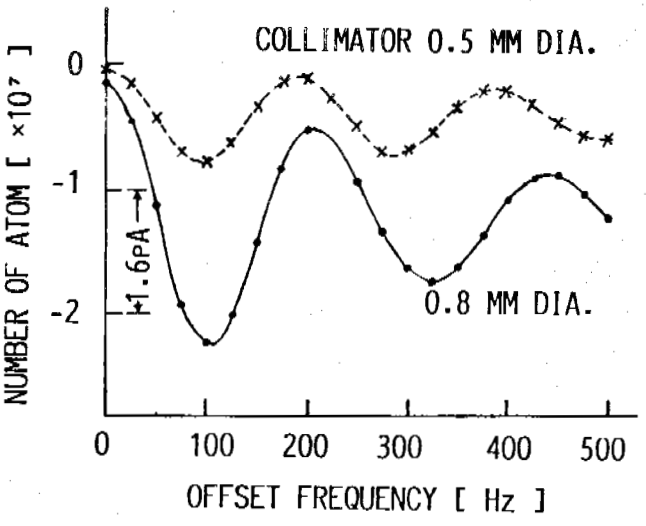

Fig. 6 Ramsey resonance for different collimators.

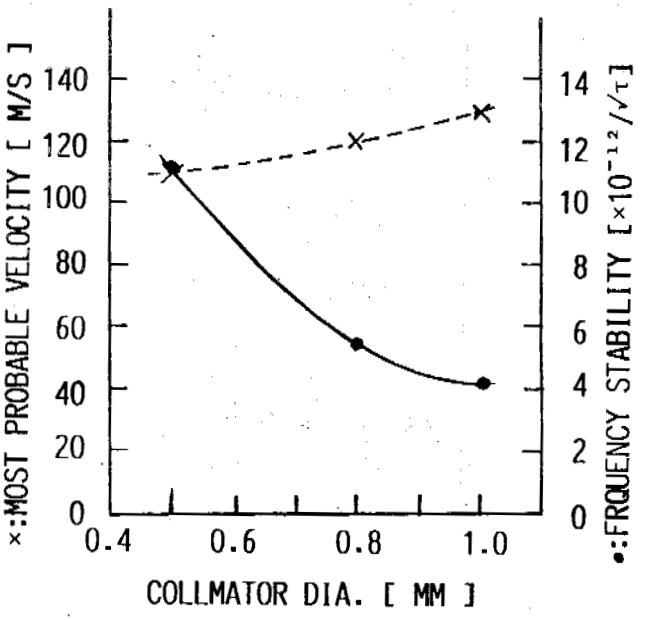

Fig. 7 Estimated short term stability and most probable velocity.

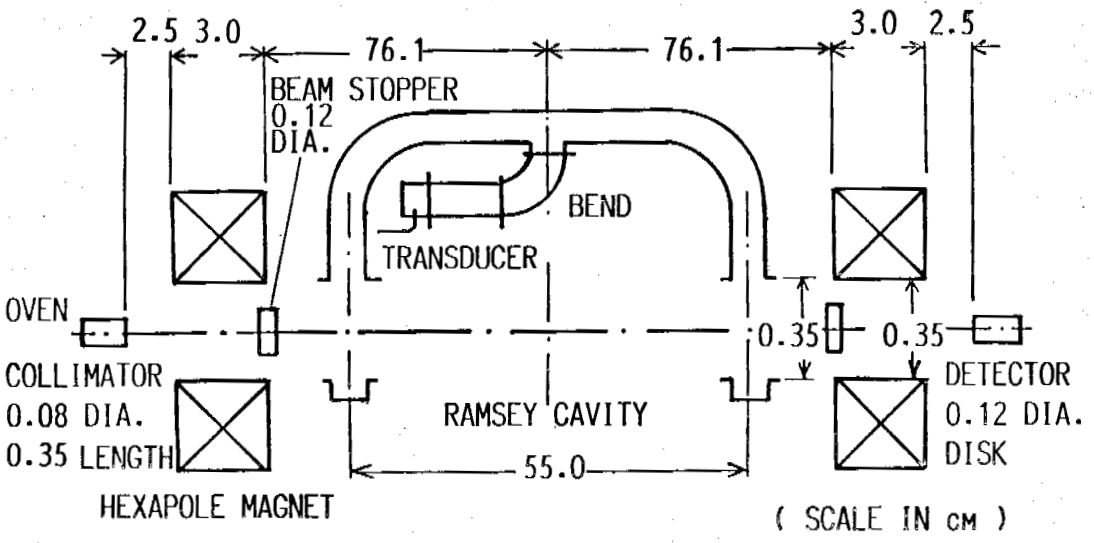

Fig. 8 Improved beam optics and the structure of Ramsey cavity.

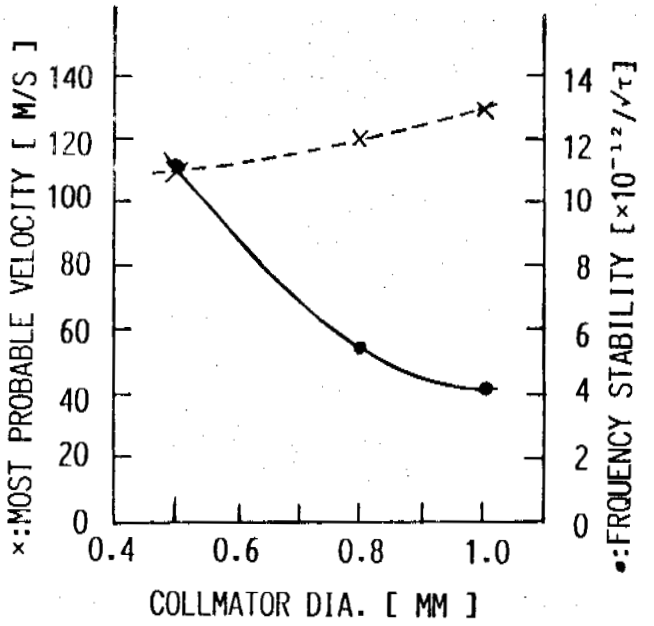

Fig. 7 Estimated short term stability and most probable velocity.

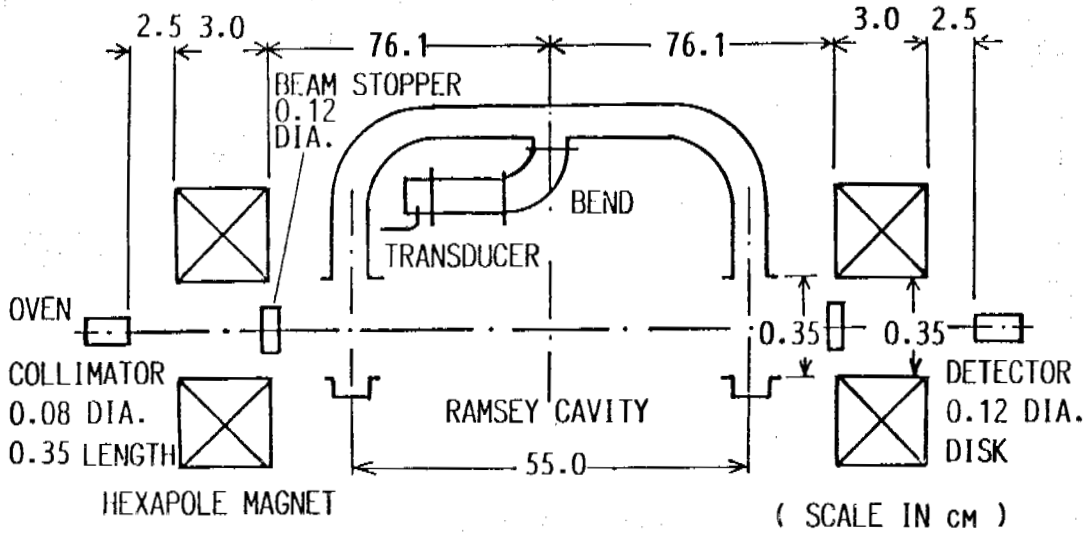

Fig. 8 Improved beam optics and the structure of Ramsey cavity.

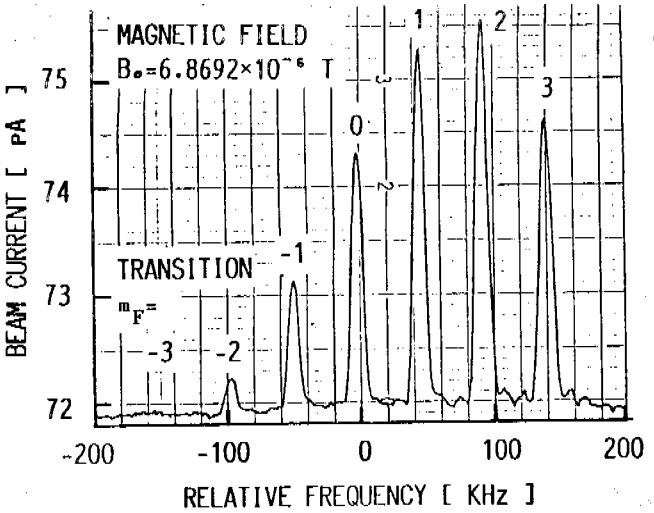

Fig. 9 Observed Rabi transitions.
transition.

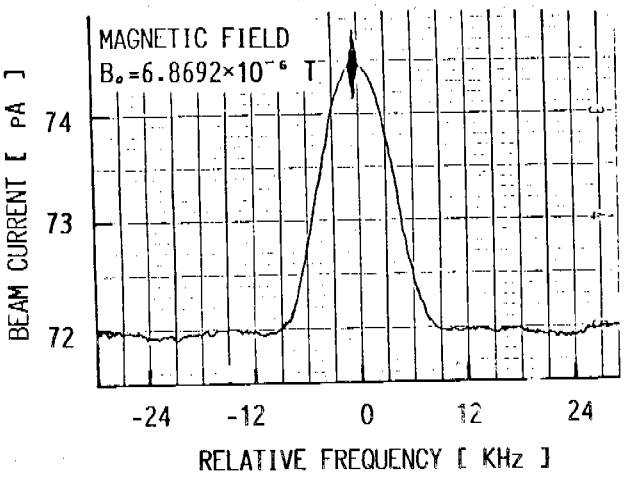

Fig. 10 Beam current arround the clock transition.

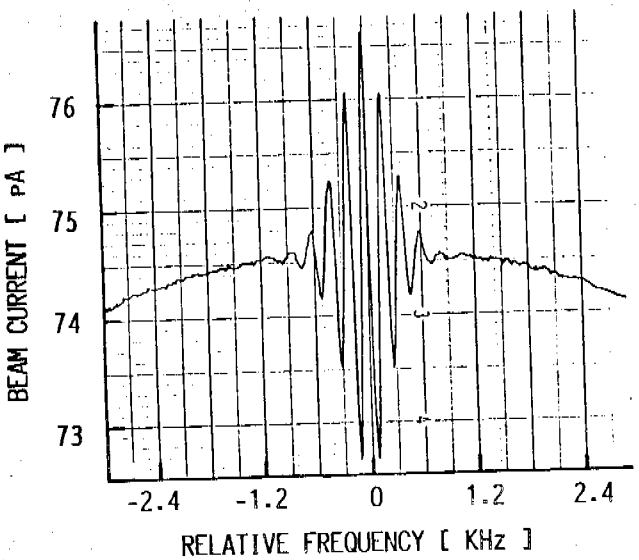

Fig. 11 Ramsey resonance of the clock transition.

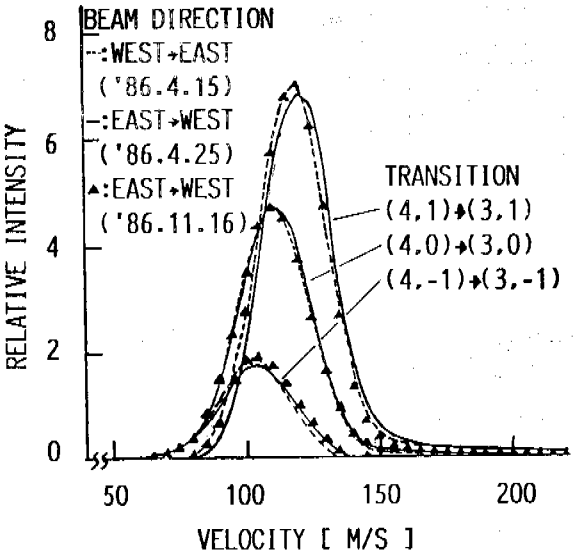

Fig. 12 Velocity distribution of three transitions.

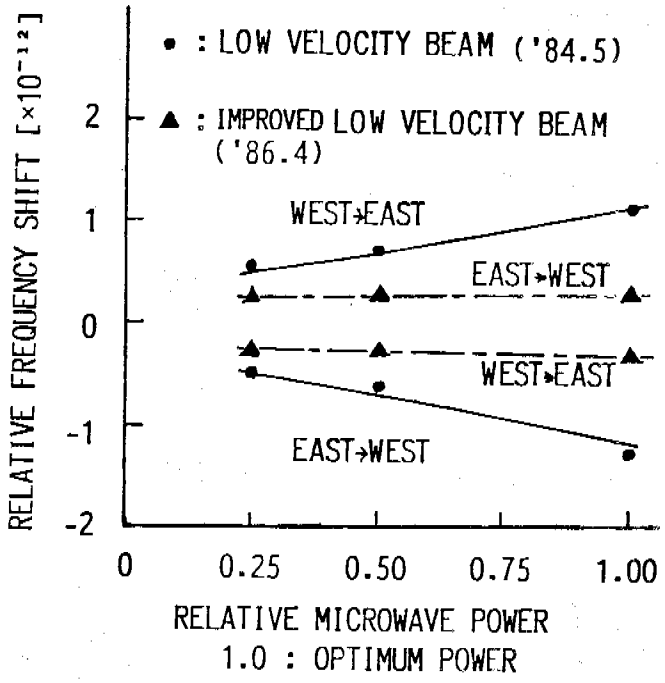

Fig. 13 Microwave power dependent characteristic on beam reversal, compared with that in the previous optics.